Appendices

Appendix 1: Basic knowledge related to x-rays

1.1. The physics of x-rays

X-rays are wave-like forms of electromagnetic energy that are carried by photons. They are characterized by a wavelength comprised of between 0.03 nm and 10 nm, which means they fall between gamma radiation and ultraviolet light on the electromagnetic spectrum. The energy associated with X-ray is usually measured in electro-volts (eV). The shorter the wavelength of an electromagnetic wave is, the higher the energy of the associated photons. For example, visible light photons have an energy of around 2eV, while X-ray photons have energies between 30 to 150keV.[1]
X-rays are classified as ionizing radiation, meaning they have the potential to interact with biological matter when they collide with it, altering its molecular bonds and producing ionisations. The process of ionisation (in which an electron is given enough energy to break away from an atom) releases energy that can damage living tissues.
There are three possible outcomes when X-rays encounter matter (Figure A1):[2]

- Transmission: once the X-ray beam hits an object it passes through it without any interaction, keeping the same direction and energy.
- Diffusion/Scattering: upon hitting the object, X-rays are reflected in different directions, without energy transfer, or with partial transfer of energy and induction of ionisation – a phenomenon known as the Compton effect.
- Absorption: the energy associated with X-ray is absorbed upon passing through an object, induction atomic ionisation – this is known as the photoelectric effect.

The production of images for medical applications is dependent on the Compton and Photoelectric effect of X-rays, which relies on ionisation and, therefore, has the potential to cause biological damage.

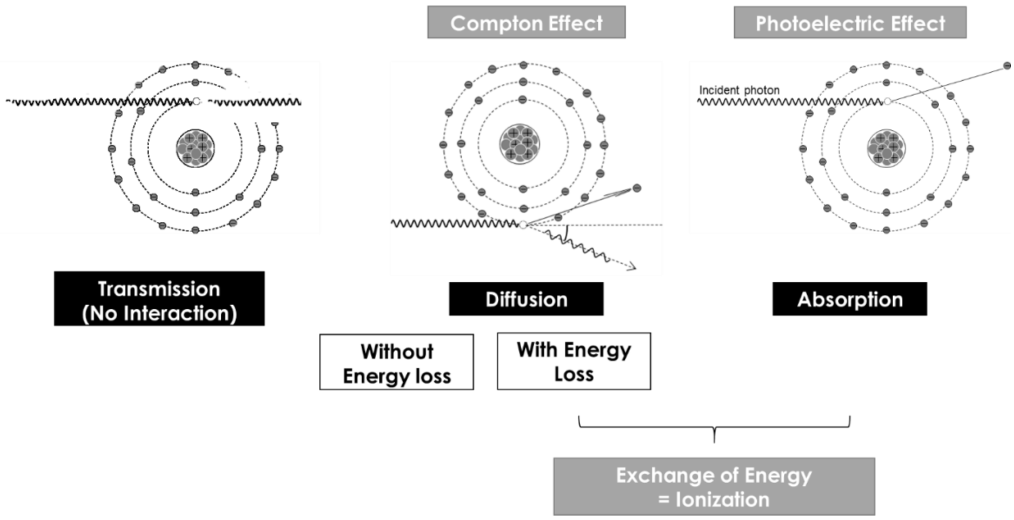

Figure A1: Main mechanisms of interaction between X-rays and matter.

1.2. X-ray production and image generation

X-ray generators (Figure A2) used in endovascular operating rooms rely on an electric current (characterized by a potential (kV)) to accelerate and induce electron collision on an anode. As much as 99% of the current's energy is transformed into heat, explaining the need for cooling systems in imaging equipment. The remaining 1% of energy is used to generate an X-ray beam that exits the X-ray tube.[3]

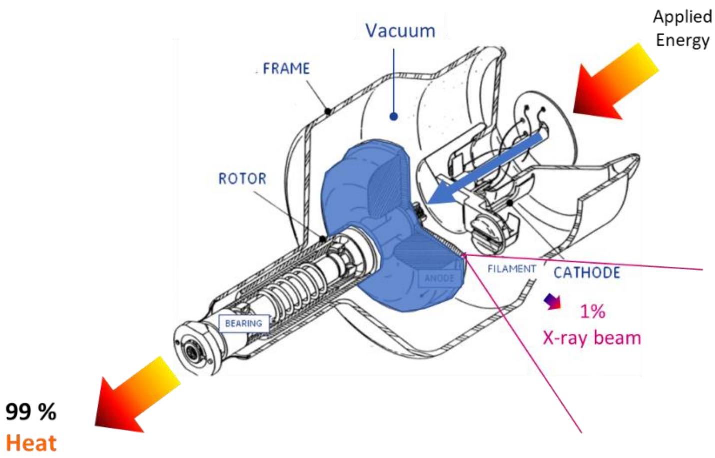

Figure A2: Example of an X-ray generator; electrons are accelerated (blue arrow) and collided on an anode (blue structure). Most of the energy is released in the form of heat, the remaining 1% forms X-rays.

The X-ray beam released travels through the operating table and the patient. Part of the beam is redirected in random directions due to the Compton effect, which accounts for scattered radiation. A proportion of the beam crosses the patient, with part of its energy being absorbed (photoelectric effect) before reaching the detector. The differences in the amount of X-ray absorbed as it passes through the body results in variable attenuation and, therefore, heterogeneous intensity of the X-rays leaving the body. Production of radiological images is ren this phenomenon.
The beam generated by X-ray machines is composed of X-rays carrying various energies (Figure A3). “Soft” X-rays carry low energy photons and are rapidly stopped by matter (absorption), they will mostly induce ionisation and are not useful for producing images.[3] “Hard” X-rays with high energy photons cross biological matter with minimal interaction also does not generate a radiological image. The “intermediate” X-rays, however, carry enough energy to allow part of the beam to cross the matter and reach the detector and the rest to be absorbed. This is the fraction of the X-ray beam that will produce images.

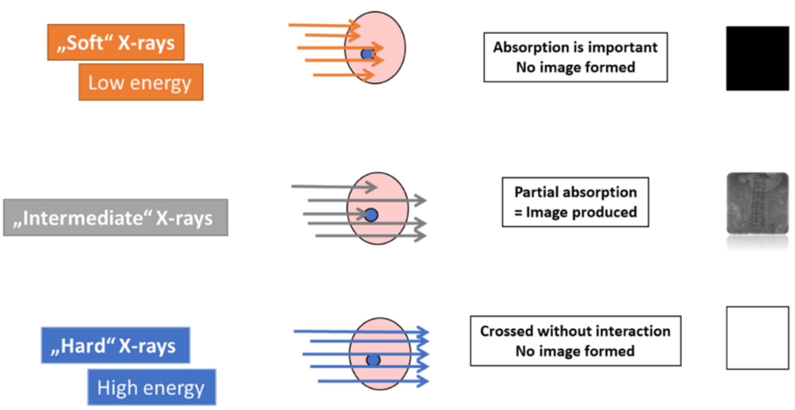

Figure A3: Differences between the X-rays produced in a generator and their role in producing an image.

Spectral filters, usually made of aluminium or copper, are positioned at the exit of the X-ray generator tube and used to stop or attenuate the low energy “soft” X-rays. Without this, the image generated by the X-ray machine would be blurred.

The filtered X-ray beam directed towards the body crosses structures that have different densities. Once the uniform X-rays enters the patient, the range of densities of the structures it crosses results in a range of attenuation, thus transforming it into a heterogenous beam,[4] that is registered as a characteristic image via the detectors (Figure A4).

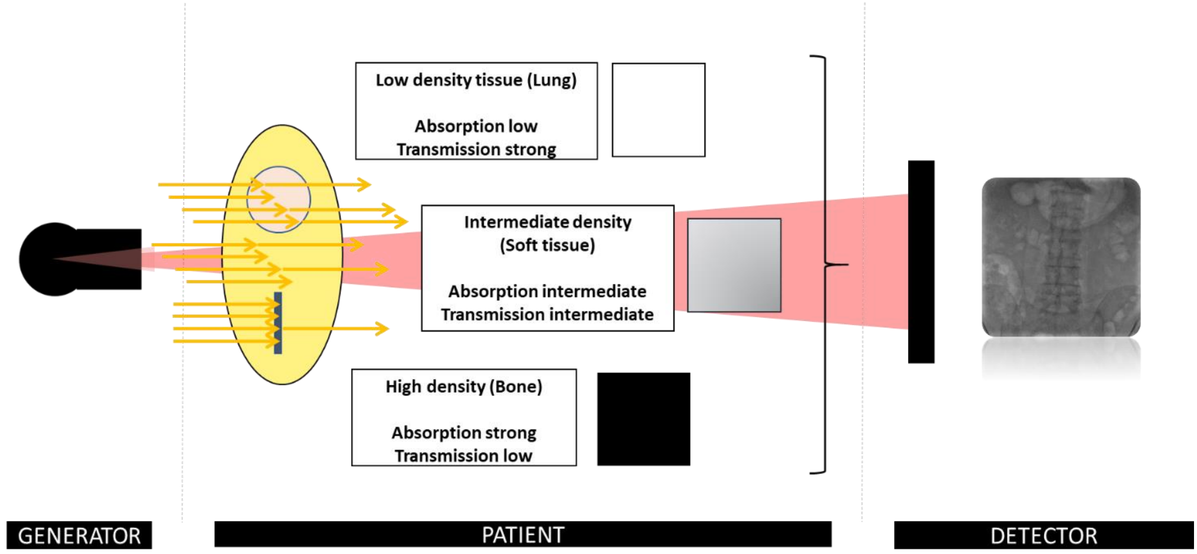

Figure A4: Image formation from the different densities of the structures crossed by the X-ray beam.

Appendix 2: Radiation exposures reported for endovascular procedures

Author	Year	Groups	Imaging System	Number of patients	KAP (Gy.cm²)	CAK (mGy)	Dose to the operator (μSv)	Dose to the staff (μSv)
De Ruiter[5]	2016		Mobile C-arm (Flat panel)	13	55.5 ± 38.9 (17.0–152.0)	300 ± 200 (100–600)	-	-
			Fixed C-arm	7	244.5 ± 142.2 (47.4–409.5)	820 ± 540 (100–1600)	-	-
			Fixed C-arm (Hybrid room)	26	157.0 ± 120.4 (25.9–418.0)	600 ± 400 (100–1600)	-	-
Antoniou[6]	2016	EVAS	Mobile C-arm	32	54 (IQR 42.1-76.8)	.	-	-
		EVAR	Mobile C-arm	32	111 (IQR 75.3-157.4)	.	-	-
Machado[7]	2016		Mobile C-arm	127	48 ± 32	.	-	-
Stansfield[8]	2016	Without preprocedure run through and brief	Fixed C-arm	61	225.11 (16.63-1671.57)	-	-	-
		With preprocedure run through and brief	Fixed C-arm	44	142.22 (20.98-635.31)	-	-	-
Nyheim[9]	2016		Fixed C-arm	80	234 (81–517)	-	-	-
Bacchim Neto[10]	2016		Fixed C-arm	30	-	-	292.6 (88.4–459.5) ¤	207.0 (73.6–407.0) ¤
Dias[11]	2016	Standard dose protocol	Fixed C-arm	25	213.83 (IQR 123.99-290.14)*	-	-	-
		Low-dose protocol, Fusion imaging	Fixed C-arm	22	98.85 (IQR 83.63-164.70)*	-	-	-
Attigah[12]	2016		Fixed C-arm (Hybrid room)	65	23 ± 25	-	620 ± 620Ɨ	470 ± 340ǂ
El-Sayed[13]	2017		Fixed C-arm	6	82.8 (53.61-144.3)	-	11 (4-74)	92 (43-203) ǂ
Tuthill[14]	2017	Centre 1	Fixed C-arm	74	77.96 ± 7.04	504.47 ± 55.07	-	-
		Centre 2		32	318.97 ± 57.97	1219.22 ± 296.48	-	-
		Centre 3		18	43.43 ± 9.94	218.09 ± 42.75	-	-

		Centre 4	Fixed C-arm (Hybrid room)	21	181.99 ± 21.41	983 ± 100.18	-	-
		Centre 5	Fixed C-arm (Hybrid room)	35	114.23 ± 13.90	790.86 ± 118.11	-	-
Stangenberg[15]	2018		Fixed C-arm (Hybrid room)	25	-	581 (116.2-2695.8)*	-	-
			Fixed C-arm	52	-	1178.5 (174.9-3351.1)*	-	-
Miller[16]	2018	Baseline	Fixed C-arm	8	-	-	120 ± 70¤	-
		Use of live dosimeters	Fixed C-arm	5	-	-	190 ± 40¤	-
			Fixed C-arm (Hybrid room)	5	-	-	30 ± 20¤	-
Ruffino[17]	2018		Fixed C-arm	25	337 (232–609)*	1608 (933–2770)*	-	-
			Fixed C-arm (Hybrid room)	25	157 (113–212)*	884 (558–1379)*	-	-
De Ruiter[18]	2018		Fixed C-arm (Hybrid room)	38	93.1 (63.5-132.5)*	400 (300-700)*	28¤	16¤
Schaefers[19]	2018		Fixed C-arm (Hybrid room)	53	168.34 ± 146.92	-	-	-
			Mobile C-arm (Flat panel)	107	49.93 (± 38.06)	-	-	-
Ahmad[20]	2018	Without Fusion	Fixed C-arm (Hybrid room)	47	32.19 (IQR 14.31–49.42)*	-	-	-
		With Fusion	Fixed C-arm (Hybrid room)	105	23.44 (IQR 15.77–51.44)*	-	-	-
Hiraoka[21]	2018	Without Fusion	Fixed C-arm (Hybrid room)	62	-	880 ± 833	-	-
		With Fusion	Fixed C-arm (Hybrid room)	81	-	768 ± 529	-	-
Maurel[22]	2018	Without cloud-based fusion (Cydar)	Fixed C-arm (Hybrid room)	21	21.7 (8.9-85.9)*	142 (61-541)*	-	-
		With cloud-based fusion (Cydar)	Fixed C-arm (Hybrid room)	33	9.17 (6.83-14.74)*	70 (45-100)*	-	-
Hertault[23]	2018		Fixed C-arm (Hybrid room)	85	14.7 (IQR 10.0-27.7)*	107 (IQR 68.0-189.0)*	-	-
Ockert[24]	2018	EVAR	Mobile C-arm (Flat panel)	30	22.6*	139*	-	-

		EVAS	Mobile C-arm (Flat panel)	30	12.4*	67.7*	-	-
Tzanis[25]	2019		Not specified	17	124.3 (41.4-627.1)*		4.7±1.4¤	
Schulz[26]	2019		Fixed C-arm (Hybrid room)	50	96.6 (±90.3)			
Kaladji[27]	2019	With cloud-based fusion (Therenva)	Mobile C-arm (Flat panel)	49	70.9 (± 48.2)			
-		Without fusion (historical cohort)	Mobile C-arm (Flat panel)	103	67.3 (± 74)			
Wermelink[28]	2019		Fixed C-arm (Hybrid room)	77	43.3* (IQR 28.4-63.3)		13 to 45¤	
Tenorio[29]	2019		Fixed C-arm (Hybrid room)	24	105 (± 116)	373 (± 257)		
Rehman[30]	2020		Mobile C-arm	78	168 (± 111)			
			Fixed C-arm (Hybrid room)	208	82 (±75)			
Våpenstad[31]	2020	Patient specific rehearsal with virtual reality	Not specified	30	12* (2.9-50.9)			
		No rehearsal	Not specified	30	13* (3.4-31.5)			
Zurcher[32]	2020	Standard imaging protocol	Fixed C-arm	17	174 (±79)	795.8 (±371.5)		
		Restricted use of angiography	Fixed C-arm	26	132 (±108)	761.4 (±721.4)		
Tzanis[33]	2020		Fixed C-arm	73	153.2*			
Harbron[34]	2020		Fixed C-arm	81	75* (IQR 48-148)			
Peters[35]	2020	EVAR	Fixed C-arm (Hybrid room)	40	278* (IQR 254-348)			

		EVAS	Fixed C-arm (Hybrid room)	67	275* (IQR 240-326)			
Martinez[36]	2020		Mobile C-arm	42	61.5 (±42.4)			
Tantawy[37]	2020	Using CO2 and CEUS	Not specified	15		182* (±135)		
Rial[38]	2020		Mobile C-arm	165	80 (±58)	307 (±257)		
Doelare[39]	2020	Without Fusion	Fixed C-arm (Hybrid room)	41	139.8 (±186.8)	694.0 (±913.8)		
-		With Fusion		20	159.1 (±102.4)	810.7 (±496.7)		
Farah[40]	2020			143	39.1 (0.1–30.1)			
Haga[41]	2020		Fixed system	172	371.3 (± 186.0)	1101 (±540)		
Kakkos[42]	2021		Mobile C-arm	48	26.8 (20.8-38.1)			
Efthymiou[43]	2021		Mobile C-arm	87	36.6* (2.0–167.8)			

Table A1: Literature review of published dose reports after EVAR between 2016 and 2022. Results are reported in means with standard deviation (SD) or (*) in median with range, or interquartile range (IQR) if stated. ¤, Dose measurement above the lead protections; ƚ, Dose to the anaesthesiologists; ǂ. ALARA : As Low As reasonably Achievable; KAP: Kerma-Area Product; CAK: Cumulative Air-kerma; CEUS: Contrast-Enhanced UltraSound; EVAR: Endovascular Aortic aneurysm Repair; EVAS: Endovascular Aortic aneurysm Sealing.

Author	Year	Groups	Imaging System	Number of patients	KAP (Gy.cm^2)	CAK (mGy)	Dose to the operator (µSv)	Dose to the staff (µSv)
Kirkwood[44]	2016		Fixed C-arm	16	601	4970	21.5	13.2
			Fixed C-arm (Hybrid room)	25	372	2580	14.1	7.1
De Ruiter[5]	2016		Fixed C-arm	15	873.8 ± 652.5 (129.7–2590)	6000 ± 4700 (800 – 18000)	-	-
			Fixed C-arm (Hybrid room)	19	598.2 ± 318.5 (128.6–1362)	3700 ± 2500 (1000–10000)	-	-
Dias[11]	2016	Standard Dose protocol (FEVAR)	Fixed C-arm	36	283.24 (IQR 192.08-499.57)*	-	-	-
		Standard Dose protocol (BEVAR)	Fixed C-arm	23	638.91 (IQR 436.96-1002.66)*	-	-	-
		Low Dose protocol and Fusion imaging (BEVAR)	Fixed C-arm	21	241.72 (IQR 140.44-432.04)*	-	-	-
		Low Dose protocol and Fusion imaging (FEVAR)	Fixed C-arm	33	262.87 (IQR 202.98-367.69)*	-	-	-
Attigah[12]	2016	FEVAR	Fixed C-arm (Hybrid room)	25	39 ± 33	-	1020 ± 1530Ɨ, 690 ± 460ǂ	-
		BEVAR	Fixed C-arm (Hybrid room)	17	48 ± 38	-	1310 ± 1580Ɨ, 700 ± 650ǂ	-
Wang[45]	2018	FEVAR	Fixed C-arm (Hybrid room)	91	-	4159 ± 2573	-	-
		Fenestrated cuff	Fixed C-arm (Hybrid room)	12	-	6063 ± 3086	-	-
De Ruiter[18]	2018		Fixed C-arm (Hybrid room)	24	384.8 (265.2-522.3)*	2900 (2000-3700)*	297¤	171¤
Manunga[46]	2018		Fixed C-arm (Hybrid room)	84	-	1097 (IQR 978-1426)*	-	-

Ruffino[17]	2018		Fixed C-arm	25	567 (388–779)*	2882 (2011–4230)*	-	-
Kirkwood[47]	2018	FEVAR	Fixed C-arm (Hybrid room)	11	210*	1800*	120*¤	60*¤
		off the shelf FEVAR	Fixed C-arm (Hybrid room)	9	280*	2200*	220*¤	110*¤
		CMD	Fixed C-arm (Hybrid room)	60	370*	2950*	370*¤	210*¤
Schanzer[48]	2020	FEVAR		732	82.8 (±158.9)	2920 (±2987)		
		Fenestrated cuff after failed EVAR		161	154.6 (±218.5)	4750 (±18,304)		
Harbron[34]	2020		Fixed C-arm	66	119* (IQR 85-209)			
Juneja[49]	2020		Mobile C-arm	11		2160 (±930.0)		
Timaran[50]	2020	With magnification	Fixed C-arm (Hybrid room)	123		2458* (IQR 1706-3767)	266* (IQR 104-583)¤	
		With digital zoom	Fixed C-arm (Hybrid room)	28		1382* (IQR 999-2045)	101* (IQR 34-235)¤	
Sen[51]	2020		Fixed C-arm (Hybrid room)	334	182 (±96)	2100 (±1800)		
Tenorio[29]	2019		Fixed C-arm (Hybrid room)	85	174 (±101)	1134 (±815)		
Doelare[39]	2020		Fixed C-arm (Hybrid room)	37	91.5 (±348.4)	2337.2 (±1744.9)		

Table A2: Literature review of published dose reports after fenestrated or branched endovascular aortic aneurysm repair (F/BEVAR) between 2016 and 2022. Results are reported in means with standard deviation (SD) or (*) in median with range, or interquartile range (IQR) if stated. ¤, Dose measurement above the lead protections; ⸸, Dose to the anaesthesiologists. ALARA: As Low As reasonably Achievable; KAP: Kerma-Area Product; CAK: Cumulative Air-kerma.

Author	Year	Anatomical Regions	Procedures	Imaging System	Number of patients	KAP (Gy.cm²)	CAK (mGy)	Dose to the operator (µSv)	Dose to the staff (µSv)
Ruiz-Cruces[52]	2016	Iliac		Fixed C-arm	48	105.7			
		Femoropopliteal	Recanalization	Fixed C-arm	57	83.9			

Maurel[53]	2017	Iliac	Patients treated in 2012	Mobile & Fixed C-arm	653	14.2 (± 18.9)			
			Patients treated in 2015	Mobile & Fixed C-arm	306	21.5 (± 37.6)			
Stangenberg[15]	2018	Femoro popliteal		Fixed C-arm	99		285.6* (IQR 152.7-486.8)		
				Fixed C-arm (Hybrid room)	35		106.0* (IQR 82.5-163.5)		
Kostova Lefterova[54]	2018	Femoro popliteal	PTA alone	Mobile C-arm	78	67* (0.6-711)			
			PTA + Stenting		20	78* (2.3-237)			
			Recanalization + PTA		39	75* (3.5-353)			
			Recanalization + stenting		52	121* (3.0-160)			
Guillou[55]	2018	Iliac	Serie n°1	Mobile C-arm	43	37.7	173.4		
			Serie n°1	Fixed C-arm	100	50	252.9		
		Femoro popliteal	Serie n°1	Mobile C-arm	56	21.5	93.8		
			Serie n°1	Fixed C-arm	99	20.2	98.1		
		Iliac & Femoro popliteal	Serie n°2	Mobile C-arm	24	19.4	66.6	0.2; 15.3¤	0.9
			Serie n°2	Fixed C-arm	76	24.2	125.8	0.3; 15.7¤	0.8
Goldsweig[56]	2019	Aortoiliac			3215	252.0 (±294.4)			
		Femoro popliteal			7203	145.6 (±212.2)			
Boc[57]	2019	Iliac	Angioplasty	Mobile C-arm	37	43.5* (IQR 28.6-87.4)			
			Stenting		161	54.9* (IQR 32.5-91.2)			
		Femoro popliteal	Angioplasty, antegrade approach		446	5.9* (IQR 4.3-8.6)			
			Angioplasty, retrograde approach		34	30.8* (IQR 22.2-48.3)			
			Stenting, antegrade approach		113	8.3* (IQR 6.0-12.3)			
			Stenting, retrograde approach		7	56.9* (20.0-93.7)			
Stahlberg[58]	2019	Iliac	With Fusion	Fixed C-arm	11	28.7* (IQR 19.7-42.2)			
			Without Fusion		15	43.8* (IQR 28.0-84.6)			

Tzanis[25]	2019	Aortoiliac		Not specified	36	23.1* (37.0-296.0)		4.4±3.6¤	
Farah[40]	2020	Iliac			130	14.4* (0.4–119.9)			
		Femoro popliteal			117	4.1* (0.1–146.8)			
Mougin[59]	2022	Iliac		Fixed C-arm	56	14*; 21.52 (±4.14)	237 (46)		
		Femoro popliteal			123	4*; 8.46 (±1.60)	80 (14)		

Table A3: Literature review of published dose reports after endovascular repair of lower extremities arterial disease between 2016 and 2020. Results are reported in means with standard deviation (SD) or (*) in median with range, or interquartile range (IQR) if stated. ¤, Dose measurement above the lead protections. ALARA: As Low As reasonably Achievable; KAP: Kerma-Area Product; CAK: Cumulative Air-kerma.

References

1. Hall E, Amato J. Giaccia, Radiobiology for the Radiologist, 6th edition. Philadelphia: Lippincott Williams & Wilkins, 2006.
2. Bushberg JT. The Essential Physics of Medical Imaging. Philadelphia: Lippincott Williams & Wilkins, 2002.
3. Russo P. Handbook of X-ray Imaging: Physics and Technology. CRC Press, 2017.
4. Hendee WR, Ritenour ER. Medical Imaging Physics. John Wiley & Sons Inc; 2003.
5. de Ruiter QMB, Moll FL, Gijsberts CM, van Herwaarden JA. AlluraClarity Radiation Dose-Reduction Technology in the Hybrid Operating Room During Endovascular Aneurysm Repair. Journal of Endovascular Therapy: An Official Journal of the International Society of Endovascular Specialists. 2016;23:130-8.
6. Antoniou GA, Senior Y, Iazzolino L, England A, McWilliams RG, Fisher RK, et al. Endovascular Aneurysm Sealing Is Associated With Reduced Radiation Exposure and Procedure Time Compared With Standard Endovascular Aneurysm Repair. Journal of Endovascular Therapy: An Official Journal of the International Society of Endovascular Specialists. 2016;23:285-9.
7. Machado R, Ferreira VMD, Loureiro L, Gonçalves J, Oliveira P, Almeida R. Radiation Exposure in Endovascular Infra-Renal Aortic Aneurysm Repair and Factors that Influence It. Brazilian Journal of Cardiovascular Surgery. 2016;31:415-21.
8. Stansfield T, Parker R, Masson N, Lewis D. The Endovascular Preprocedural Run Through and Brief: A Simple Intervention to Reduce Radiation Dose and Contrast Load in Endovascular Aneurysm Repair. Vasc Endovascular Surg. 2016;50:241-6.
9. Nyheim T, Staxrud LE, Jørgensen JJ, Jensen K, Olerud HM, Sandbæk G. Radiation exposure in patients treated with endovascular aneurysm repair: what is the risk of cancer, and can we justify treating younger patients? Acta Radiol. 2017;58:323-30.
10. Bacchim Neto FA, Alves AF, Mascarenhas YM, Nicolucci P, Pina DR. Occupational radiation exposure in vascular interventional radiology: A complete evaluation of different body regions. Phys Med. 2016;32:1019-24.
11. Dias NV, Billberg H, Sonesson B, Törnqvist P, Resch T, Kristmundsson T. The effects of combining fusion imaging, low-frequency pulsed fluoroscopy, and low-concentration contrast agent during endovascular aneurysm repair. J Vasc Surg. 2016;63:1147-55.

12. Attigah N, Oikonomou K, Hinz U, Knoch T, Demirel S, Verhoeven E, et al. Radiation exposure to eye lens and operator hands during endovascular procedures in hybrid operating rooms. J Vasc Surg. 2016;63:198-203.
13. El-Sayed T, Patel AS, Cho JS, Kelly JA, Ludwinski FE, Saha P, et al. Radiation-Induced DNA Damage in Operators Performing Endovascular Aortic Repair. Circulation. 2017;136:2406-16.
14. Tuthill E, O'Hora L, O'Donohoe M, Panci S, Gilligan P, Campion D, et al. Investigation of reference levels and radiation dose associated with abdominal EVAR (endovascular aneurysm repair) procedures across several European Centres. Eur Radiol. 2017;27:4846-56.
15. Stangenberg L, Shuja F, Bom IMJvd, Alfen MHGv, Hamdan AD, Wyers MC, et al. Modern Fixed Imaging Systems Reduce Radiation Exposure to Patients and Providers. Vasc Endovascular Surg. 2018;52:52-8.
16. Miller C, Kendrick D, Shevitz A, Kim A, Baele H, Jordan D, et al. Evaluating strategies for reducing scattered radiation in fixed-imaging hybrid operating suites. J Vasc Surg. 2018;67:1227-33.
17. Ruffino MA, Fronda M, Discalzi A, Isoardi P, Bergamasco L, Ropolo R, et al. Radiation dose during endovascular aneurysm repair (EVAR): upgrade of an angiographic system from standard to Eco mode. Radiol Med. 2018;123:966 -- 72.
18. de Ruiter QMB, Jansen MM, Moll FL, Hazenberg CEVB, Kahya NN, van Herwaarden JA. Procedure and step-based analysis of the occupational radiation dose during endovascular aneurysm repair in the hybrid operating room. J Vasc Surg. 2018;67:1881-90.
19. Schaefers JF, Wunderle K, Usai MV, Torsello GF, Panuccio G. Radiation doses for endovascular aortic repairs performed on mobile and fixed C-arm fluoroscopes and procedure phase-specific radiation distribution. J Vasc Surg. 2018;68:1889-96.
20. Ahmad W, Obeidi Y, Majd P, Brunkwall JS. The 2D-3D Registration Method in Image Fusion Is Accurate and Helps to Reduce the Used Contrast Medium, Radiation, and Procedural Time in Standard EVAR Procedures. Ann Vasc Surg. 2018;51:177-86.
21. Hiraoka A, Shiraya S, Chikazawa G, Ishida A, Miyake K, Sakaguchi T, et al. Feasibility of three-dimensional fusion imaging with multimodality roadmap system during endovascular aortic repair. J Vasc Surg. 2018;68:1175-82.
22. Maurel B, Martin-Gonzalez T, Chong D, Irwin A, Guimbretière G, Davis M, et al. A prospective observational trial of fusion imaging in infrarenal aneurysms. J Vasc Surg. 2018;68:1706-13.e1.
23. Hertault A, Rhee R, Antoniou GA, Adam D, Tonda H, Rousseau H, et al. Radiation Dose Reduction During EVAR: Results from a Prospective Multicentre Study (The REVAR Study). Eur J Vasc Endovasc Surg. 2018;56:426-33.
24. Ockert S, Heinrich M, Kaufmann T, Syburra T, Lopez R, Seelos R. Endovascular aortic sealing with Nellix reduces intraoperative radiation dose when compared to endovascular aortic repair. J Vasc Surg. 2018;67:1068-73.
25. Tzanis E, Tsetis D, Kehagias E, Ioannou CV, Damilakis J. Occupational exposure during endovascular aneurysm repair (EVAR) and aortoiliac percutaneous transluminal angioplasty (PTA) procedures. Radiol Med. 2019;124:539 -- 45.
26. Schulz CJ, Bockler D, Krisam J, Geisbusch P. Two-dimensional-three-dimensional registration for fusion imaging is noninferior to three-dimensional- three-dimensional registration in infrarenal endovascular aneurysm repair. J Vasc Surg. 2019;70:2005-13.
27. Kaladji A, Villena A, Pascot R, Lalys F, Daoudal A, Clochard E, et al. Fusion Imaging for EVAR with Mobile C-arm. Ann Vasc Surg. 2019;55:166-74.
28. Wermelink B, Willigendael EM, Smit C, Beuk RJ, Brusse-Keizer M, Meerwaldt R, et al. Radiation exposure in an endovascular aortic aneurysm repair program after introduction of a hybrid operating theater. J Vasc Surg. 2019;70:1927-34 e2.

29. Tenorio ER, Oderich GS, Sandri GA, Ozbek P, Karkkainen JM, Vrtiska T, et al. Prospective nonrandomized study to evaluate cone beam computed tomography for technical assessment of standard and complex endovascular aortic repair. J Vasc Surg. 2020;71:1982-93 e5.
30. Rehman ZU, Choksy S, Howard A, Carter J, Kyriakidis K, Elizabeth D, et al. Comparison of Patient Radiation Dose and Contrast Use during EVAR in a Dedicated Hybrid Vascular OR and Mobile Imaging. Ann Vasc Surg. 2019;61:278-83.
31. Vapenstad C, Lamoy SM, Aasgaard F, Manstad-Hulaas F, Aadahl P, Sovik E, et al. Influence of patient-specific rehearsal on operative metrics and technical success for endovascular aneurysm repair. Minim Invasive Ther Allied Technol. 2021;30:195-201.
32. Zurcher KS, Naidu SG, Money SR, Stone WM, Fowl RJ, Knuttinen G, et al. Dose reduction using digital fluoroscopy versus digital subtraction angiography in endovascular aneurysm repair: A prospective randomized trial. J Vasc Surg. 2020;72:1938-45.
33. Tzanis E, Ioannou CV, Tsetis D, Lioudaki S, Matthaiou N, Damilakis J. Complexity-based local diagnostic reference levels (DRLs) for standard endovascular aneurysm repair (EVAR) procedures. Phys Med. 2020;73:89-94.
34. Harbron RW, Abdelhalim M, Ainsbury EA, Eakins JS, Alam A, Lee C, et al. Patient radiation dose from x-ray guided endovascular aneurysm repair: a Monte Carlo approach using voxel phantoms and detailed exposure information. J Radiol Prot. 2020;40:704-26.
35. Peters AS, Hatzl J, Bischoff MS, Bockler D. Comparison of endovascular aneurysm sealing and repair with respect to contrast use and radiation in comparable patient cohorts. J Cardiovasc Surg (Torino). 2020;61:67-72.
36. Martinez LI, Esteban C, Riera C, Altes P, Llagostera S. Endovascular Infrarenal Aortic Aneurysm Repair Performed in a Hybrid Operating Room Versus Conventional Operating Room Using a C-Arm. Ann Vasc Surg. 2020;69:366-72.
37. Tantawy TG, Seriki D, Rogers S, Katsogridakis E, Ghosh J. Endovascular Aneurysm Repair Assisted by CO2 Digital Subtraction Angiography and Intraoperative Contrast-Enhanced Ultrasonography: Single-Center Experience. Ann Vasc Surg. 2021;70:459-66.
38. Rial R, Vañó E, Río-Solá MLD, Fernández JM, Sánchez RM, Santervás LAC, et al. National Diagnostic Reference Levels for Endovascular Aneurysm Repair and Optimisation Strategies. Eur J Vasc Endovasc Surg. 2020;60:837-42.
39. Doelare SAN, Smorenburg SPM, van Schaik TG, Blankensteijn JD, Wisselink W, Nederhoed JH, et al. Image Fusion During Standard and Complex Endovascular Aortic Repair, to Fuse or Not to Fuse? A Meta-analysis and Additional Data From a Single-Center Retrospective Cohort. J Endovasc Ther. 2021;28:78-92.
40. Farah J, Gonzalez-Mendez LA, Dufay F, Amir S, Royer B, Gabriel H, et al. Patient exposure and diagnostic reference levels in operating rooms: a multi-centric retrospective study in over 150 private and public French clinics. J Radiol Prot. 2020.
41. Haga Y, Chida K, Sota M, Kaga Y, Abe M, Inaba Y, et al. Hybrid Operating Room System for the Treatment of Thoracic and Abdominal Aortic Aneurysms: Evaluation of the Radiation Dose Received by Patients. Diagnostics (Basel). 2020;10.
42. Kakkos SK, Efthymiou FO, Metaxas VI, Dimitroukas CP, Panayiotakis GS. Factors affecting radiation exposure in endovascular repair of abdominal aortic aneurysms: a pilot study. Int Angiol. 2021;40:125-30.
43. Efthymiou FO, Metaxas VI, Dimitroukas CP, Kakkos SK, Panayiotakis GS. Kerma-Area Product, Entrance Surface Dose and Effective Dose in Abdominal Endovascular Aneurysm Repair. Radiat Prot Dosimetry. 2021;194:121-34.
44. Kirkwood ML, Guild JB, Arbique GM, Tsai S, Modrall JG, Anderson JA, et al. New image-processing and noise-reduction software reduces radiation dose during complex endovascular procedures. J Vasc Surg. 2016;64:1357-65.

45. Wang SK, Drucker NA, Sawchuk AP, Lemmon GW, Dalsing MC, Motaganahalli RL, et al. Use of the Zenith Fenestrated platform to rescue failing endovascular and open aortic reconstructions is safe and technically feasible. J Vasc Surg. 2018;68:1017-22.
46. Manunga J, Sullivan T, Garberich R, Alden P, Alexander J, Skeik N, et al. Single-center experience with complex abdominal aortic aneurysms treated by open or endovascular repair using fenestrated/branched endografts. J Vasc Surg. 2018;68:337-47.
47. Kirkwood ML, Chamseddin K, Arbique GM, Guild JB, Timaran D, Anderson JA, et al. Patient and operating room staff radiation dose during fenestrated/branched endovascular aneurysm repair using premanufactured devices. J Vasc Surg. 2018;68:1281 -- 6.
48. Schanzer A, Beck AW, Eagleton M, Farber MA, Oderich G, Schneider D, et al. Results of fenestrated and branched endovascular aortic aneurysm repair after failed infrarenal endovascular aortic aneurysm repair. J Vasc Surg. 2020;72:849-58.
49. Juneja A, Zia S, Ayad MH, Singh K, Dietch J, Schor J. Safety and Feasibility of Performing Fenestrated Endovascular Abdominal Aneurysm Repair Using a Portable C-arm Without Fusion Technology: A Single-Center Experience. Cureus. 2020;12:e7739.
50. Timaran LI, Timaran CH, Scott CK, Soto-Gonzalez M, Timaran-Montenegro DE, Guild JB, et al. Dual fluoroscopy with live-image digital zooming significantly reduces patient and operating staff radiation during fenestrated-branched endovascular aortic aneurysm repair. J Vasc Surg. 2021;73:601-7.
51. Sen I, Tenorio ER, Pitcher G, Mix D, Marcondes GB, Lima GBB, et al. Effect of obesity on radiation exposure, quality of life scores, and outcomes of fenestrated-branched endovascular aortic repair of pararenal and thoracoabdominal aortic aneurysms. J Vasc Surg. 2021;73:1156-66 e2.
52. Ruiz-Cruces R, Vano E, Carrera-Magarino F, Moreno-Rodriguez F, Soler-Cantos MM, Canis-Lopez M, et al. Diagnostic reference levels and complexity indices in interventional radiology: a national programme. Eur Radiol. 2016;26:4268-76.
53. Maurel B, Hertault A, Mont LSd, Cazaban S, Rinckenbach S. A Multicenter Survey of Endovascular Theatre Equipment and Radiation Exposure in France during Iliac Procedures. Ann Vasc Surg. 2017;40:50-6.
54. Kostova-Lefterova DD, Nikolov NN, Stanev SS, Stoyanova BB. Patient doses in endovascular and hybrid revascularization of the lower extremities. Br J Radiol. 2018;91:20180176.
55. Guillou M, Maurel B, Necib H, Vent P-A, Costargent A, Chaillou P, et al. Comparison of Radiation Exposure during Endovascular Treatment of Peripheral Arterial Disease with Flat-Panel Detectors on Mobile C-arm versus Fixed Systems. Ann Vasc Surg. 2018;47:104-13.
56. Goldsweig AM, Kennedy KF, Abbott JD, Jones WS, Velagapudi P, Rutar FJ, et al. Patient Radiation Dosage During Lower Extremity Endovascular Intervention. JACC Cardiovasc Interv. 2019;12:473-80.
57. Boc V, Boc A, Zdesar U, Blinc A. Patients' radiation doses during percutaneous endovascular procedures in arteries of the lower limbs. Vasa. 2019;48:167-74.
58. Stahlberg E, Sieren M, Anton S, Jacob F, Planert M, Barkhausen J, et al. Fusion Imaging Reduces Radiation and Contrast Medium Exposure During Endovascular Revascularization of Iliac Steno-Occlusive Disease. Cardiovasc Intervent Radiol. 2019;42:1635-43.
59. Mougin J, Louis N, Maupas E, Goueffic Y, Fabre D, Haulon S. Fusion imaging guidance for endovascular recanalization of peripheral occlusive disease. J Vasc Surg. 2022;75:610-7.